Applied Physics Letters

High-quality InP nanoneedles grown on silicon

Cite as: Appl. Phys. Lett. **102**, 012115 (2013); https://doi.org/10.1063/1.4775377
Submitted: 10 November 2012 . Accepted: 21 December 2012 . Published Online: 11 January 2013

Fan Ren (任凡), Kar Wei Ng (吳嘉偉), Kun Li (李琨), Hao Sun (孙皓), and Connie J. Chang-Hasnain

AIP Publishing

High-quality InP nanoneedles grown on silicon

Fan Ren (任凡), Kar Wei Ng (吴嘉偉), Kun Li (李琨), Hao Sun (孙皓), and Connie J. Chang-Hasnain[a)]
Department of Electrical Engineering and Computer Sciences, University of California at Berkeley, Berkeley, California 94720, USA

(Received 10 November 2012; accepted 21 December 2012; published online 11 January 2013)

In this letter, we report the growth of self-assembled, catalyst-free InP nanoneedles on Si substrate by low-temperature metal-organic chemical vapor deposition. With a characteristic core-shell growth mode, the nanostructure size is scalable with growth time, and InP/InGaAs/InP double-heterostructure is demonstrated. Single crystalline wurtzite InP nanoneedles essentially free of stacking faults and polytypism are achieved. The internal quantum efficiency of as-grown unpassivated InP nanoneedles can reach as high as 15% at room temperature. Laser oscillation is realized from single InP nanoneedle under optical pump. These promising results reveal the potential of integrating InP nanoneedle optoelectronic devices with traditional silicon. © *2013 American Institute of Physics*. [http://dx.doi.org/10.1063/1.4775377]

Bottom-up approach of integrating III-V compound semiconductors on silicon has attracted intense interest because it enables bridging of the gap between optoelectronic devices and silicon-based complementary metal-oxide-semiconductor (CMOS) circuits.[1–3] However, large mismatches in lattice constants and thermal coefficients hinder direct growth of III-V materials on silicon. Nanostructures with small footprints grown on Si substrate give a possible solution. But the nanowires usually have small lateral dimensions[4] and require metal catalyst.[5,6] These often degrade the material quality and restrict their applications. Recently, we reported a core-shell growth mechanism which enables monolithic growth of high-quality GaAs-based nanoneedles and nanopillars directly on silicon and realized high-performance single-nanopillar lasers.[7–9] This showed an approach to overcome the fundamental roadblock due to lattice mismatch between III-V compound semiconductor and silicon.

Among all the III-V materials, InP is one of the most important building blocks for realizing heterojunction devices. In fact, InP based alloys are widely used as growth template, optical cladding layers, and active layers in long wavelength optoelectronic devices for silicon-transparent applications. Most importantly, InP has 1–2 orders of magnitude lower surface recombination velocity than GaAs-based materials.[10,11] These unique properties make InP an ideal candidate for surface passivation as well as solar cell application.[12] InP nanowires grown on silicon have been reported using gold or indium as catalyst. However, single crystalline phase can only be observed when nanowire diameter is smaller than a critical diameter below 40 nm.[4,13,14] In this letter, we report the growth of catalyst-free, self-assembled InP nanoneedles on silicon by low-temperature metal-organic chemical vapor deposition (MOCVD). With a core-shell growth mode, the InP nanoneedle can grow up to ~1.2 μm in diameter. Transmission electron microscopy (TEM) studies show that these gigantic structures grown at 450 °C are in single crystalline wurtzite (WZ) phase. With the use of temperature-dependent photoluminescence (PL), the internal quantum efficiency (IQE) of unpassivated nanoneedle is measured to be as high as 15% at room temperature. Lasing behavior is observed at 4 K under pulsed optical pump, attesting the excellent crystal quality. InP/InGaAs/InP double-heterostructure (DH) is also demonstrated, suggesting the possibility of integration of long wavelength heterojunction devices on silicon.

Material growth was carried out on (111)-Si substrates in an Emcore D75 MOCVD system. Trimethylindium (TMIn) and tertiarybutylphosphine (TBP) were adopted as indium and phosphorus precursors, respectively. Prior to growth, the Si substrates were cleaned with acetone, methanol and rinsed with DI water in sequence. The substrate surface was then deoxidized by dipping into buffered oxide etch, followed by mechanical roughening.[7] TBP was flown into the reactor when substrate temperature was higher than 200 °C. A pre-growth *in-situ* annealing was performed at 540 °C for 3 min. Reactor temperature was then lowered and kept at the growth temperature, which ranged from 400 to 450 °C. TMIn was introduced into the reactor afterward to prevent self-catalyst effect of indium at low temperature. The total flow rate during the growth was fixed as 12 slm. The mole fractions of TBP and TMIn were held as 2.36×10^{-3} and 1.89×10^{-5}, respectively.

Figures 1(a)–1(d) show the scanning electron microscope (SEM) images of typical InP nanoneedles grown at 425 °C and 450 °C for 15 min. At both growth temperatures, the nanoneedles are well-faceted hexagonal pyramids aligning vertically to Si [111] direction. The InP [11$\bar{2}$0] direction is parallel to Si [1$\bar{1}$0] direction. The nanoneedles grown at 425 °C possess straight sidewalls and a typical taper angle of 2.5°–3.5°, as observed in Fig. 1(b). However, the ones grown at 450 °C show curved sidewalls and significantly larger base with diameter as large as ~1.2 μm, as shown in Fig. 1(d). This is possibly due to enhanced indium surface migration at higher temperature. Therefore, more indium can be collected from surface and incorporate at base part of the nanoneedles.[15]

To study the InP nanoneedle growth mechanism, five samples were grown at 425 °C with growth time ranging

[a)]Electronic mail: cch@eecs.berkeley.edu.

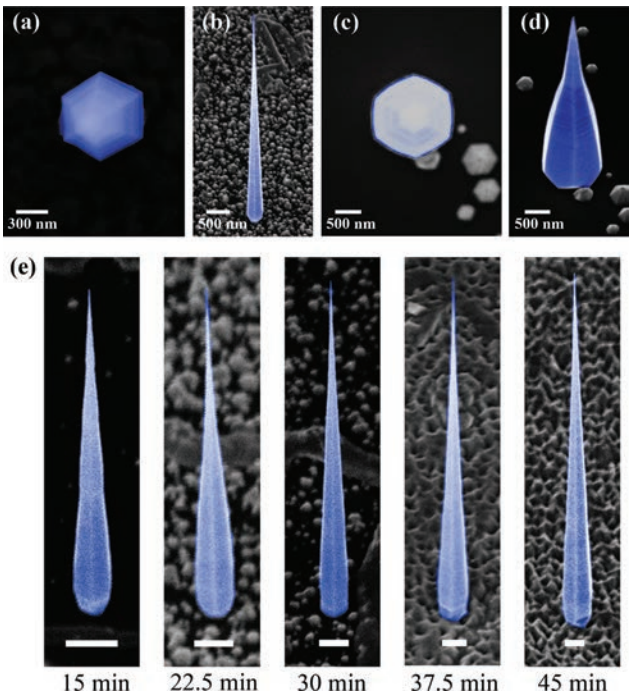

FIG. 1. SEM images of InP nanoneedles on (111)-Si substrate. (a) and (b) Top view and 30°-tilt view of InP nanoneedles grown at 425 °C for 15 min, respectively. (c) and (d) Top view and 30°-tilt view of InP nanoneedles grown at 450 °C for 15 min, respectively. (e) Size evolution of nanoneedles with different growth times. Scale bars are 500 nm.

from 15 to 45 min. The size evolution of nanoneedles with growth time is shown in Fig. 1(e). The nanoneedle taper angle is well maintained with base diameter and height scaling linearly with time. The vertical and lateral growth rates along $[1\bar{1}00]$ and [0001] orientations are estimated to be 16.7 nm·min^{-1} and 360 nm·min^{-1}, respectively. No critical diameter or height for InP nanoneedle on silicon was observed despite 8% lattice-mismatch between these two materials. Similar shape evolution was also observed at 450 °C. This behavior indicates that InP nanoneedle growth is in a core-shell mode rather than the vapor-liquid-solid growth mechanism usually observed for conventional nanowires.[1,3]

To further prove that the growth indeed assumes core-shell mode, InP/$In_{0.2}Ga_{0.8}As$/InP DH was demonstrated. The InP core diameter is designed as 450 nm, while both of the InGaAs layer and InP shell thicknesses are chosen as 100 nm. The structural schematic and 30°-tilt SEM image of the nanopillar are shown in Figs. 2(a) and 2(b), respectively. It is considered that the flat top results from the InGaAs layer growth. In our previous work, it is observed that the InGaAs nanoneedles are truncated when its length exceeds 1.5 μm.[16] Due to the growth condition variation across the sample surface, some short nanopillars with a height of ~320 nm are also found. InGaAs layer is exposed on the top of those short nanopillars. The InGaAs layer can be removed by selective wet etching while leaving InP layers intact, resulting in a trench between two InP layers, as shown in Figure 2(c). The measured thicknesses of InGaAs intermediate layer and InP shell agree with the designed ones. Two smooth boundaries of the trench can be seen at the original InGaAs/InP interfaces. It indicates that good interfaces are formed between the

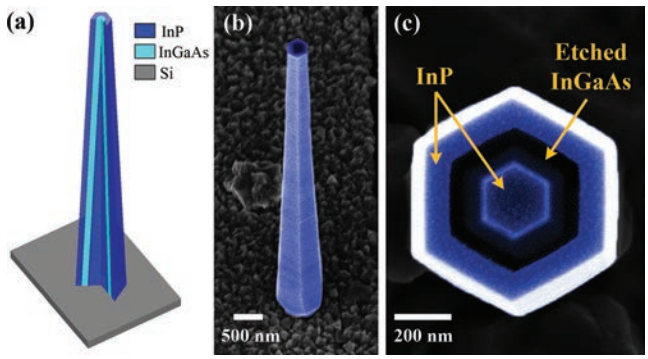

FIG. 2. Nanopillar with InP/InGaAs/InP double-heterostructure. (a) Schematic illustrating the core-shell structure of the nanopillar. (b) 30°-tilt SEM image of InP/InGaAs/InP nanopillar. (c) Top-down view of a nanopillar with InGaAs layer removed by selective etching.

two materials. Furthermore, suggested by the excellent appearance of outer interfaces, the 100-nm-thick InGaAs layer could grow with a good crystal quality, despite over 2% lattice-mismatch respect to InP. The ability of growing DH further confirms that the InP nanoneedle growth follows a core-shell manner. Furthermore, it also reveals a potential approach to integrate high-performance optoelectronic devices in silicon transparency range monolithically with silicon.

To study the crystal phase and material quality of the nanoneedles, high-resolution TEM (HR-TEM) was performed. TEM sample was prepared by simply wiping down as-grown InP nanoneedles onto a TEM copper grid. Figures 3(a) and 3(b) show the TEM images of InP nanoneedles grown at 425 °C and 450 °C, respectively. The corresponding diffraction patterns (DPs) inserted in Fig. 3(a) and shown in Fig. 3(d) match the distinctive WZ pattern. It confirms that both 425 °C and 450 °C can offer WZ crystalline phase.

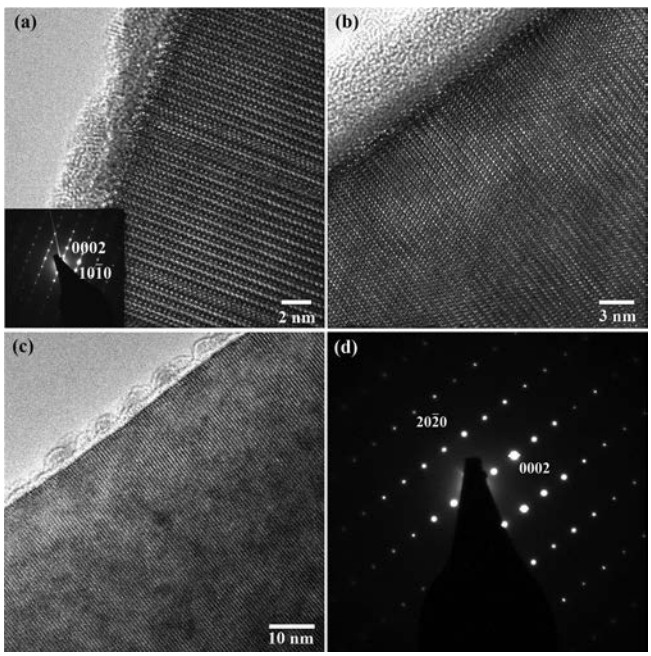

FIG. 3. (a) A HR-TEM image of a 425 °C InP nanoneedle, with FFT inserted. (b) A HR-TEM image of a 450 °C InP nanoneedle. (c) A zoom-out TEM image of a 450 °C InP nanonneedle. No stacking fault or polytypism are observed over 100 nm along c-direction. (d) Diffraction pattern of a 450 °C InP nanoneedle.

However, small zinc blende (ZB) phase portions are observed in the TEM image of the ample grown at 425 °C, resulting in the streaky components in the corresponding DP. In contrast, for the sample grown at 450 °C, neither stacking fault nor polytypism was observed within a large area over 100 nm along the nanoneedle. This feature as well as the clear diffraction pattern verifies that the growth temperature of 450 °C can improve crystalline phase purity significantly. It is believed that the basic crystal phase is determined by the nucleus crystal structure, considering the InP nanoneedle has a coherent core-shell growth mode. WZ phase is energetically favorable due to a lower dangling bond density on the sidewalls,[17] since the initial nucleus is small and the surface-to-volume ratio is large. Therefore, under both growth temperatures, WZ structure can be formed at initial growth stage and maintained by the core-shell growth mode. However, in terms of thermal dynamics, the formation of stacking fault is possible during the growth. It is because the ZB structure is more energetically preferred, when the nanoneedle size increases and surface-to-volume ratio reduces.[18,19] We anticipate that the actual V/III ratios under the two growth temperatures can be the key factor for crystal phase control in our experiments. In fact, the actual V/III ratio increases due to higher TBP pyrolysis efficiency at 450 °C.[20] It could have affected the surface energy at growth front and nucleation kinetics. Higher V/III ratio leads to a higher supersaturation at growth surface, which makes ZB crystal phase less favorable.[21] As a result, in our experiments, pure WZ structure is realized at 450 °C, while ZB structure appears at 425 °C. Similar phenomenon has been observed, showing a higher V/III ratio can suppress the formation of ZB in InP nanowire growth.[22] To fully verify and understand the effect of V/III ratio on crystal structure, further experimental and theoretical studies are both needed for following research.

Optical properties characterization was carried out for the single, as-grown pure WZ InP nanoneedles. The material IQE was evaluated by temperature dependent PL with temperature varying between 4 K and room temperature.[23] A continuous-wave semiconductor laser emitting at 660 nm was used as the pump source. The pump power ranged from 50 μW to 10 mW at each temperature. The full-width-at-half-maximum (FWHM) of pump laser spot was focused down to 2.3 μm. The temperature depending IQE curve is plotted in Fig. 4. The WZ InP nanoneedle shows an IQE of 15% at room temperature despite the unpassivated surface. This value is significantly lower than that of bulk InP, which can reach over 90%.[24] It is mainly attributed to the relatively large surface-to-volume ratio. The carriers in nanoneedle have high probability to diffuse to the surface before radiative recombination. Surface states act as nonradiative recombination centers and the IQE is reduced. However, it is worth noting that the IQE of our uncoated InP nanoneedle is surprisingly two times higher than the previous best reported 5% from GaAs nanowire with InGaP passivation layer.[25] We attribute this amazing efficiency mainly to the lower surface recombination velocity of InP, larger base size, and relatively smaller surface-to-volume ratio, comparing with other nanowires. This makes InP nanoneedle on silicon a good candidate for low-cost and high-efficiency solar cell application. The negative thermal quenching is also observed when

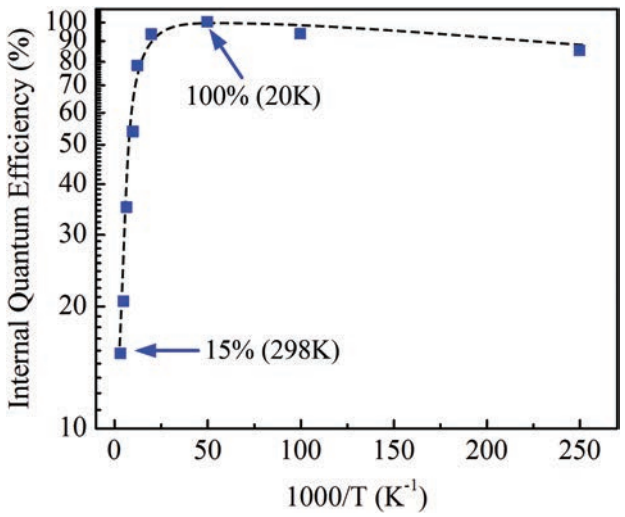

FIG. 4. IQE measurement data of a 450 °C InP nanoneedle, extracted from power-dependent PL measurements under different temperatures. An IQE of 15% at room temperature is achieved.

the temperature is lower than 20 K. The mechanism of this behavior from our WZ InP is not clear yet. Similar phenomena were observed from GaAs, ZnS and ZnO materials. It could be due to intermediate energy states formed by impurities, such as hydrogen and carbon, or intrinsic point defects.[26,27]

The InP nanoneedle tapered shape can provide a natural optical cavity supporting unique helically propagating resonance modes.[8] The resonance wavelengths can be tuned by nanoneedle diameters to match the InP material emission spectrum. With high material quality mentioned above and this excellent as-grown cavity, laser oscillation was achieved at 4 K under optical pump. A mode-locked Ti:sapphire laser (Coherent Chamelleon) delivering 140 fs pulses was used as the pump source. The pump wavelength was fixed at 750 nm with a repetition rate of 80 MHz. The FWHM of pump laser spot was focused down to 2.5 μm. The emission spectra of a WZ InP nanoneedle laser at 4 K are plotted in Fig. 5(a). A background suppression ratio of 8.6 dB was measured from lasing spectrum. Figure 5(b) shows the laser output-input curve (L-L curve) for a typical WZ InP nanolaser. The pump power and nanoneedle laser emission are both converted into energy per area. A clear threshold behavior can be seen in the L-L curve. The emission linewidth becomes narrower rapidly as the pump power increases towards threshold. The lasing peak broadening above threshold is due to the heating effect. By fitting the curve with a gain model and rate equations, the nanoneedle laser threshold is evaluated as $\sim$7.3 μJ·cm^{-2}. The cavity quality factor (Q) and the spontaneous emission coupling factor (β) are estimated as $\sim$126 and $\sim$0.021, respectively. This demonstrates the potential of integrating these InP nanoneedle lasers onto silicon for various applications, such as on-chip and inter-chip connection for CMOS.

In conclusion, we report the catalyst-free, self-assembled, core-shell growth of InP nanoneedles on 8% lattice-mismatched (111)-Si substrate. InP nanoneedles grown at 450 °C are in single crystalline WZ phase and essentially free of stacking fault. InP/InGaAs/InP DH was also demonstrated. The IQE of as-grown InP nanoneedle is as high as 15%. With the naturally formed cavity, laser

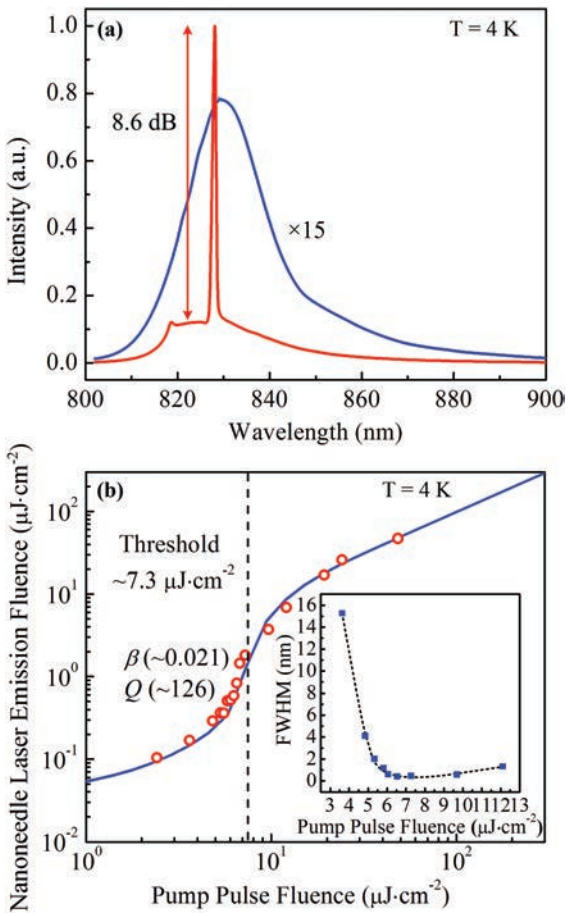

FIG. 5. (a) PL spectrum of a single WZ InP nanoneedle laser below (blue, magnified by 15) and above (red) threshold at 4 K. (b) L-L curve of a nanoneedle laser operating at 4 K, fitted with gain model and rate equations. A low threshold of $\sim 7.3\,\mu J \cdot cm^{-2}$, a cavity quality factor (Q) of ~126, and spontaneous emission coupling factor (β) of ~0.021 are estimated from rate equation analysis, respectively. The linewidth reduces by a factor of 10 as the pump increases above the threshold, shown in the inset.

oscillation from single InP nanoneedle on silicon was achieved. These exciting properties make the nanoneedles attractive for low-cost, high-efficiency solar cell application, as well as open up a pathway for silicon-transparent optoelectronic devices integrated with silicon.

This work was supported by U.S. DOE SunShot Program via contract DE-EE0005316, DoD NSSEFF Fellowship via contract N00244-09-1-0013 and N00244-09-1-0080, and California Advanced Solar Technologies Institute, UC Multicampus Research Program and Initiatives (MRPI). The authors acknowledge the support of the National Center for Electron Microscopy, Lawrence Berkeley Laboratory for the use of their facilities.

[1]M. Moewe, L. C. Chuang, S. Crankshaw, K. W. Ng, and C. Chang-Hasnain, Opt. Express **17**, 7831 (2009).
[2]K. Tomioka, Y. Kobayashi, J. Motohisa, S. Hara, and T. Fukui, Nanotechnology **20**, 145302 (2009).
[3]L. C. Chuang, M. Moewe, S. Crankshaw, and C. Chang-Hasnain, Appl. Phys. Lett. **92**, 013121 (2008).
[4]L. C. Chuang, M. Moewe, C. Chase, N. P. Kobayashi, and C. Chang-Hasnain, Appl. Phys. Lett. **90**, 043115 (2007).
[5]G. E. Cirlin, V. G. Dubrovskii, Y. B. Samsonenko, A. D. Bouravleuv, K. Durose, Y. Y. Proskuryakov, B. Mendes, L. Bowen, M. A. Kaliteevski, R. A. Abram, and D. Zeze, Phys. Rev. B **82**, 035302 (2010).
[6]Y. Watanabe, H. Hibino, S. Bhunia, K. Tateno, and T. Sekiguchi, Physica E **24**, 133 (2004).
[7]M. Moewe, L. C. Chuang, S. Crankshaw, C. Chase, and C. Chang-Hasnain, Appl. Phys. Lett. **93**, 023116 (2008).
[8]R. Chen, T. D. Tran, K. W. Ng, W. S. Ko, L. C. Chuang, F. G. Sedgwick, and C. Chang-Hasnain, Nat. Photon. **5**, 170 (2011).
[9]F. Lu, T. D. Tran, W. S. Ko, K. W. Ng, R. Chen, and C. Chang-Hasnain, Opt. Express **20**, 12171 (2012).
[10]S. Bothra, S. Tyagi, S. K. Chandhi, and J. M. Borrego, Solid State Electron. **34**, 47 (1991).
[11]D. E. Aspnes, Surf. Sci. **132**, 406 (1983).
[12]C. J. Keavney, V. E. Haven, and S. M. Vernon, in *Conference Record of the Twenty First IEEE Photovoltaic Specialists Conference*, Kissimimee, FL, USA, 21-25 May 1990 (IEEE, New York, 1990), pp. 141–144.
[13]G. E. Cirlin, V. G. Dubrovskii, I. P. Soshnikov, N. V. Sibirev, Y. B. Samsonenko, A. D. Bouravleuv, J. C. Harmand, and F. Glas, Phys. Status Solidi (RRL) **3**, 112 (2009).
[14]E. Ertekin, P. A. Greaney, D. C. Chrzan, and T. D. Sands, J. Appl. Phys. **97**, 114325 (2005).
[15]V. G. Dubrovskii, M. V. Nazarenko, L. C. Chuang, W. S. Ko, K. W. Ng, and C. Chang-Hasnain, Appl. Phys. Lett. **98**, 153113 (2011).
[16]K. W. Ng, W. S. Ko, T. D. Tran, R. Chen, M. V. Nazarenko, F. Lu, V. G. Dubrovskii, M. Kamp, A. Forchel, and C. J. Chang-Hasnain, "Unconventional growth mechanism for monolithic integration of III–V on silicon," ACS Nano (in press).
[17]X. Ren, H. Huang, V. G. Dubrovskii, N. V. Sibirev, M. V. Nazarenko, A. D. Bolshakov, X. Ye, Q. Wang, Y. Huang, X. Zhang, J. Guo, and X. Liu, Semicond. Sci. Technol. **26**, 014034 (2011).
[18]T. Akiyama, K. Sano, K. Nakamura, and T. Ito, Jpn. J. Appl. Phys., Part 2 **45**, L275 (2006).
[19]F. Glas, J. C. Harmand, and G. Patriarche, Phys. Rev. Lett. **99**, 146101 (2007).
[20]C. H. Chen, C. A. Larsen, G. B. Stringfellow, D. W. Brown, and A. J. Robertson, J. Cryst. Growth **77**, 11 (1986).
[21]V. G. Dubrovskii, N. V. Sibirev, J. C. Harmand, and F. Glas, Phys. Rev. B **78**, 235301 (2008).
[22]S. Paiman, Q. Gao, H. H. Tan, C. Jagadish, K. Pemasiri, M. Montazeri, H. E. Jackson, L. M. Smith, J. M. Yarrison-Rice, X. Zhang, and J. Zou, Nanotechnology **20**, 225606 (2009).
[23]S. Watanabe, N. Yamada1, M. Nagashima, Y. Ueki, C. Sasaki, Y. Yamada, T. Taguchi, K. Tadatomo, H. Okagawa, and H. Kudo, Appl. Phys. Lett. **83**, 4906 (2003).
[24]H.-J. Schimper, Z. Kollonitsch, K. Möller, U. Seidel, U. Bloeck, K. Schwarzburg, F. Willig, and T. Hannappel, J. Cryst. Growth **287**, 642 (2006).
[25]C. P. T. Svensson, T. Mårtensson, J. Trägårdh, C. Larsson, M. Rask, D. Hessman, L. Samuelson, and J. Ohlsson, Nanotechnology **19**, 305201 (2008).
[26]H. Shibata, Jpn. J. Appl. Phys., Part 1 **37**, 550 (1998).
[27]M. Watanabe, M. Sakai, H. Shibata, C. Satou, S. Satou, T. Shibayama, H. Tampo, A. Yamada, K. Matsubara, K. Sakurai, S. Ishizuka, S. Niki, K. Maeda, and I. Niikura, Physica B **376–377**, 711 (2006).